The International Journal of Advanced Manufacturing Technology (2024) 133:811–820
https://doi.org/10.1007/s00170-024-13684-8

ORIGINAL ARTICLE

Effect of current waveform in MIG arc on weld bead formation in plasma-MIG hybrid welding

Kazuya Ishida[1,2] · Shinichi Tashiro[1] · Kazufumi Nomura[3] · Dongsheng Wu[1] · Anthony B. Murphy[4] · Toshifumi Yuji[5] · Manabu Tanaka[1]

Received: 31 December 2023 / Accepted: 22 April 2024 / Published online: 24 May 2024

Abstract
Plasma-metal inert gas (MIG) hybrid welding enables to join thick steel plates in single pass. However, arc coupling occurring between the plasma and MIG arcs disturbs its heat source characteristics, lowering the welding quality. This arc coupling phenomenon is not yet understood due to the complexity. This study aims to clarify the effect of current waveform of arc on weld bead formation according to the arc coupling in plasma-MIG hybrid welding. The metal transfer characteristics and bottom side weld pool were observed for direct current (DC) and pulse-MIG current waveforms. In addition, Ni element was used for visualizing the transport process of high-temperature molten metal provided by MIG welding within the weld pool. From these results, the effects of differences in MIG arc current waveforms on heat and mass transport processes within the weld pool and also on weld bead formation on the bottom side through changes in the occurrence of arc coupling were discussed. As a result, it was clarified that the droplets after detachment from the wire were transferred to the weld pool surface under the wire tip for DC MIG current, while those were transferred along the wire axis to the weld pool surface behind the keyhole for pulse-MIG current. When the droplet was transferred to the weld pool region with the forward flow such as the pulse-MIG current case, the heat was transported to the bottom side together with the counter-clockwise eddy behind the keyhole, strongly contributing to increasing the penetration depth. In the case of pulse-MIG current, the plasma arc is oscillated due to the arc coupling. According to this oscillation, the accumulation of molten metal behind the keyhole is prevented to suppress the humping bead formation. Consequently, pulse-MIG current was found to be suitable for increasing the penetration depth and suppressing humping bead formation on the bottom side comparing with DC MIG current.

Keywords Hybrid welding · Plasma welding · MIG welding · Arc coupling · Droplet · Humping bead

1 Introduction

Today's manufacturing industry demands high-quality welding in short time and at low investment costs for various materials [1, 2]. When multilayer welding is performed using gas metal arc (GMA) welding on the widely used high-strength steel, preheating and inter-pass temperature control are required. However, if high-strength steel can be welded in single pass, there will be no need to control the temperature between passes, which will shorten the work time. To solve this problem, research is actively underway into welding methods with high heat flux to achieve deep penetration. One method is the application of hybrid welding process. Particularly, laser-arc hybrid welding is being put into practical use in industry [3–5]. In addition, plasma-GMA hybrid welding is also suitable because the plasma welding equipment is much cheaper than the laser welding equipment and has many advantages such as easy installation and high root gap tolerance [6–8]. Therefore, it is expected to be an alternative process to the laser-arc hybrid welding in future.

In the plasma-GMA hybrid welding, plasma welding is used in the leading position, and a keyhole is formed in the

✉ Shinichi Tashiro
tashiro.shinichi.jwri@osaka-u.ac.jp

1 Joining and Welding Research Institute (JWRI), Osaka University, 11-1 Mihogaoka, Ibaraki, Osaka 567-0047, Japan

2 Morita Corporation, Osaka, Japan

3 Division of Materials and Manufacturing Science, Graduate School of Engineering, Osaka University, Ibaraki, Japan

4 CSIRO Manufacturing, Sydney, Australia

5 University of Miyazaki, Miyazaki, Japan

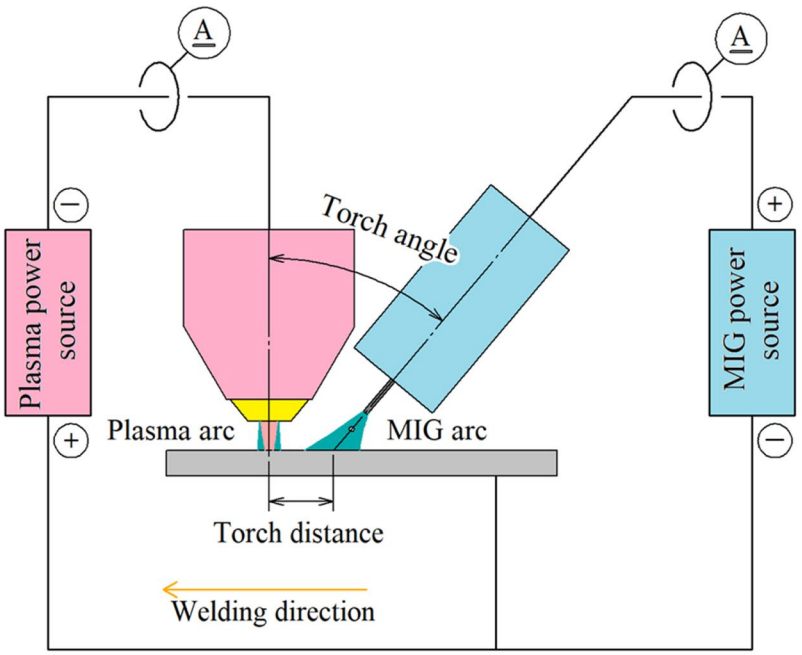

Fig. 1 Schematic diagram of the experimental setup of the plasma-MIG hybrid welding and the welding conditions

Plasma welding		MIG welding	
Shielding gas	Pure Ar/ 15 l/min	Shielding gas	Pure Ar/ 15 l/min
Pilot gas	Pure Ar/ 2.5 l/min	Wire diameter	φ1.2 mm
Arc length	7 mm	CTWD	20 mm
Welding speed	40 cm/min		
Root gap	1.5 mm		
Torch angle	30°		
Torch distance	25 mm		

weld pool due to a high arc pressure and a large heat flux brought by the constricted plasma arc, and full penetration until the bottom surface is achieved [9, 10]. Then, GMA welding in the trailing position produces metal droplets by melting the welding wire, filling the keyhole and gap with the droplets at a high deposition rate. Plasma welding and GMA welding are welding processes that have been extensively studied for a long time. When these are used as hybrid welding, electromagnetic interference (defined as "arc coupling" in this paper) occurs between the two arcs. For this reason, each process exhibits heat source characteristics and convection in the weld pool which cannot be seen in individual processes.

Recently, various research was carried out for clarifying the arc coupling phenomenon and also effect on the welding process. Ishida et al. applied through 3D spectroscopic measurements of plasma temperature and iron vapor concentration fields to plasma-metal inert gas (MIG) welding to discuss the arc coupling mechanism [11]. MIG welding is a type of GMA welding and uses argon as a shielding gas. It was found that when a direct current (DC) was used for MIG arc, the plasma arc and MIG arc were continuously coupled to stably form a direct current path between two arcs. On the other hand, in a pulse-MIG current case, this arc coupling occurred only in the upslope duration of pulse current. Wu et al. observed both arcs in plasma-MIG welding with a high-speed video camera, showing that when the direct current path was formed between the arcs, the MIG current path from the wire to the weld pool was expanded, and droplet detachment was prompted [12]. They then performed a weld pool simulation to evaluate the flow pattern of the weld pool

Table 1 Current and voltage conditions

	Plasma setting current (A)	MIG setting current (A)	MIG setting voltage (V)
DC-MIG	260	230	25
Pulse-MIG	240	170	24

Table 2 Chemical compositions of base metal and wire (wt.%)

	C	Si	Mn	P	S	Cr	Ni	Mo	V	Ti	Cu	Al	Nb	B	N	Fe
Base metal	0.14	0.3	1.15	0.011	0.001	0.3	0.07	0.167	0.011	0.009	0.1	0.037	0.001	0.001	0.002	Bal.
Wire	0.09	0.32	1.05	0.008	0.01	0.24	2.71	0.49	-	-	-	-	-	-	-	Bal.

and the driving force to induce the flow [13]. In addition, the transport process of heat and mass provided by droplets in the weld pool was also clarified [14]. Yu et al. challenged to manage the arc coupling phenomenon with application of external magnetic field for controlling metal transfer. It was found that the metal transfer mode was significantly affected by the plasma current via the arc coupling. The duration of arc coupling enables to be controlled by the external magnetic field [15]. The influence of the external magnetic field on welded bead was also clarified, proving that the mechanical properties of the welded bead were improved by applying the magnetic field [16]. Although fragmentary knowledge about the arc coupling is obtained through research conducted using various approaches to date, systematical understanding, for example the interaction between arc and weld pool considering the arc coupling, has not yet been acquired.

As mentioned above, one of the most important features of plasma-GMA hybrid welding is the arc coupling between the plasma arc and GMA. It is becoming increasingly clear that this has a strong influence not only on the heat source characteristics of the arc, but also on the metal transfer characteristics and the weld pool formation process. One of the major welding defects that often occurs during this welding process is the formation of a humping bead on the bottom surface, which is also seen in laser-GMA hybrid welding [17]. This defect depends on the heat and mass transport processes within the weld pool, so the arc coupling is thought to have a large influence on it, but the details are still not understood. In this study, plasma-MIG hybrid welding is used. The metal transfer characteristics and bottom side weld pool are observed when the MIG current waveform is DC and DC pulse. In addition, the Ni element mainly contained in the welding wire is used as a tracer to visualize the transport process of high-temperature molten metal supplied by MIG welding within the weld pool. From these results, we will clarify the effects of differences in MIG arc current waveforms on the heat and mass transport processes within the weld pool and also on the weld bead formation on the bottom side through changes in the occurrence of arc coupling.

2 Experimental procedure

Figure 1 shows a schematic diagram of experimental setup of the plasma-MIG hybrid welding and the welding conditions. A transfer-type plasma welding torch (NW-504WH, Nippon steel Welding & Engineering), a plasma welding power source (NW-300ASR, Nippon Steel Welding & Engineering), a MIG welding torch (WT3500, Daihen), a MIG inverter pulse welding power source (DP 350, Daihen Co., Ltd.), and a wire feeder (CM-7401, Daihen) are used. A diameter of the water-cooled copper nozzle of plasma welding torch is 3.2 mm. The plasma welding torch and MIG welding torch are installed at the leading and trailing positions, respectively. The angle between the two torches is 30°. The arc length, which is the distance from the plasma torch nozzle to the base metal surface, is 7 mm, and the MIG welding wire extension length is 20 mm. The distance between the central axes of the two torches on the base metal

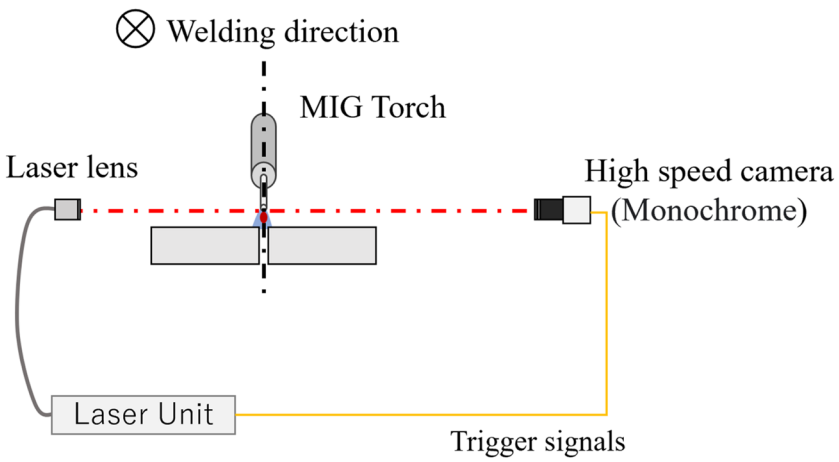

Fig. 2 High-speed camera arrangement for metal transfer shooting

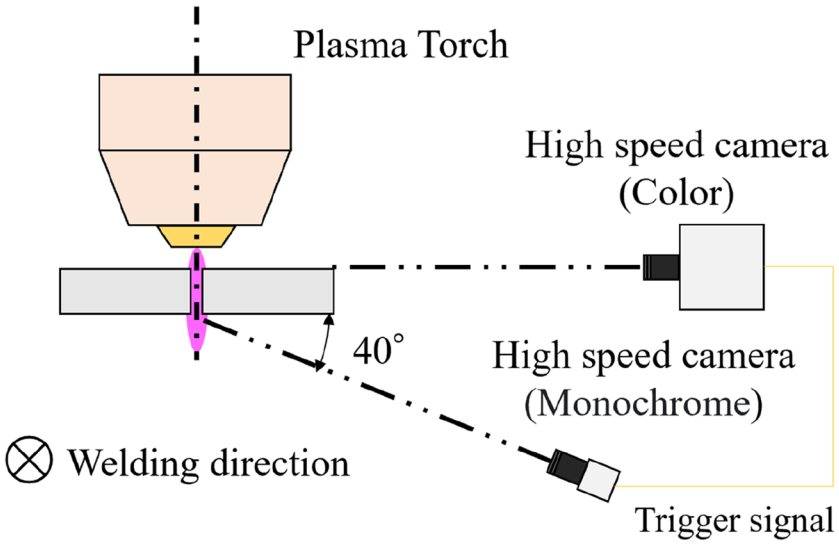

Fig. 3 Schematic of the simultaneous observation system for the arc phenomenon and the bottom weld pool

is 25 mm. Pure argon is used for the pilot gas and shielding gas for plasma welding and the shielding gas for MIG welding, whose flowrates are 2.5, 15, and 15 L/min, respectively. The welding velocity is 40 cm/min.

Table 1 shows the current and voltage conditions. In this study, DC current and DC pulse current are used as the MIG current for plasma-MIG hybrid welding. The condition of the MIG current with the DC waveform is expressed as "DC-MIG," and that with the DC pulse waveform is expressed as "Pulse-MIG." Depending on the welding conditions, a root humping may occur [17]. Since the currents of MIG welding for both current waveforms are selected to prevent occurrence of root humping, the currents of plasma welding are different. An example of current waveform for the pulse-MIG current is presented in Fig. 10 later.

Table 2 shows the chemical compositions of the base metal and wire. The base metal is 780-MPa grade high-strength steel (STRENX700E, SSAB). The wire used for MIG welding is JIS Z3312 G78A4MN5CM3T (MG-S80, KOBELCO) for 780 MPa class with a diameter of 1.2 mm. The contents of C, P, and S are lower than those of standard carbon steel. The welding wire contains 2.7% Ni, which is much higher than 0.07% in the base metal, so it is possible to confirm whether the wire components have melted into the weld zone by Ni element mapping. The specimen dimensions are 6 mm thick, 50 mm wide, and 300 mm long, and an I groove with a root gap of 1.5 mm is applied.

Figure 2 shows a schematic of the droplet transfer observation system for plasma-MIG hybrid welding using the shadow graph method. A high-speed camera (Memrecam Q1v, Nac Image Technology) is placed on one side of the welding torch, and a pulsed laser system (Cavilux HF, Cavitar) with a wavelength of 640 nm is placed on the other side. In the observation, a shutter speed of 4000 fps, an exposure time of 20 µs, and a lens aperture of F32 are selected. Neutral density (ND) filters are installed in front of the camera lens for reducing the brightness of light. By sending the

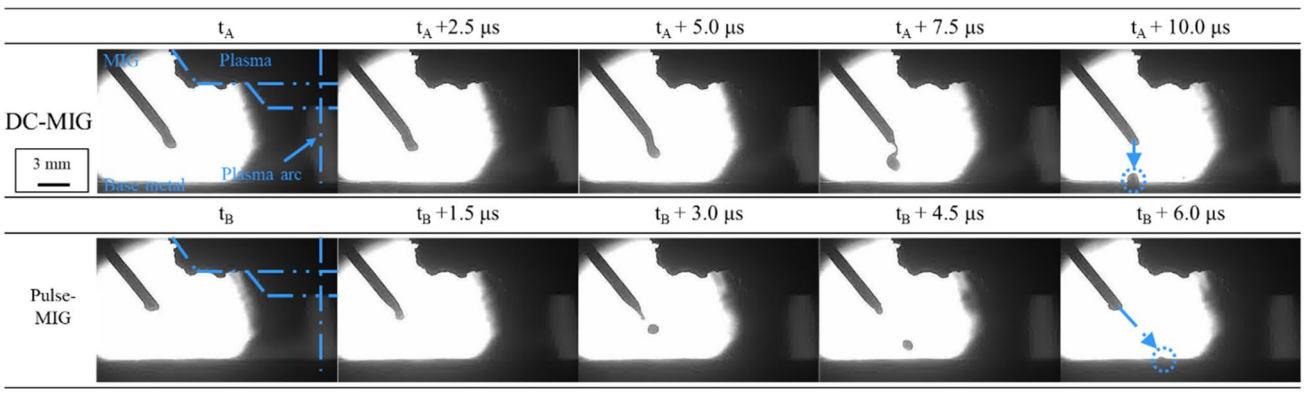

Fig. 4 Time sequential images of metal transfer behavior for DC-MIG current and pulse-MIG current during plasma-MIG hybrid welding

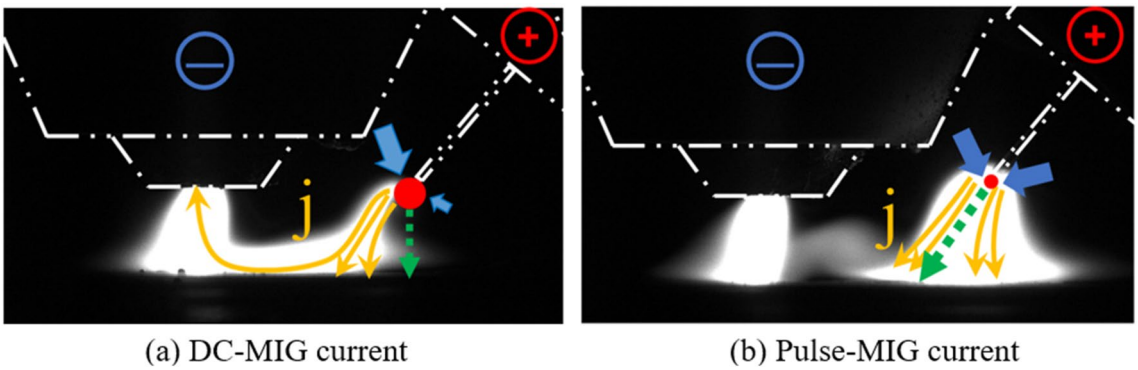

Fig. 5 Arc appearances and expected current paths for DC-MIG current and pulse-MIG current during plasma-MIG hybrid welding

trigger signal of the high-speed camera to the laser system, the timings of pulse laser irradiation and the camera shutter are synchronized.

Figure 3 shows a schematic of the simultaneous observation system for the arc phenomenon and the bottom weld pool. A color high-seed camera (ACS-1 M60, Nac Image Technology) for observing the arc phenomenon is placed horizontally with the base metal, and the arc above the base metal surface and the efflux plasma flowing out to the bottom side through the keyhole are simultaneously observed. In addition to the above, the efflux plasma and the weld bead on bottom side are also observed simultaneously by a monochrome high-speed camera (Memrecam Q1v-V-209-M8, Nac Image Technology). The start signal of color camera observation is sent to the monochrome camera as the trigger signal for the synchronization. The observation conditions for the color camera are a frame rate of 2000 fps, an exposure time of 10 μs, and a lens aperture of F32. A neutral density (ND) filter is installed in front of the camera lens for reducing the light intensity. The observation conditions for the monochrome camera are a frame rate of 2000 fps, an exposure time of 497 μs, and a lens aperture of F32.

3 Results and discussion

3.1 Effect of MIG current waveform on heat and mass transport processes in weld pool

Figure 4 shows the time sequential images of metal transfer behavior for DC-MIG current and pulse-MIG current during plasma-MIG hybrid welding. It was found that droplets after detachment from the wire were transferred to the weld pool surface under the wire tip for DC-MIG current, while those were transferred along the wire axis to the weld pool surface behind the keyhole for pulse-MIG current.

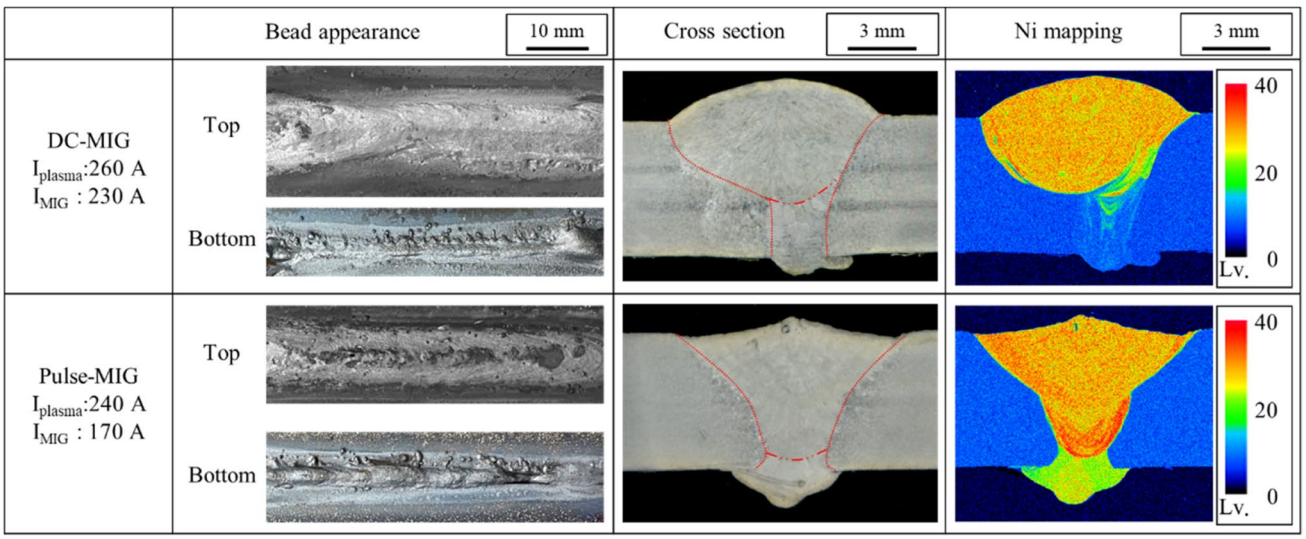

Fig. 6 Bead appearances, cross-sections, and Ni element distributions for DC-MIG current and pulse-MIG current

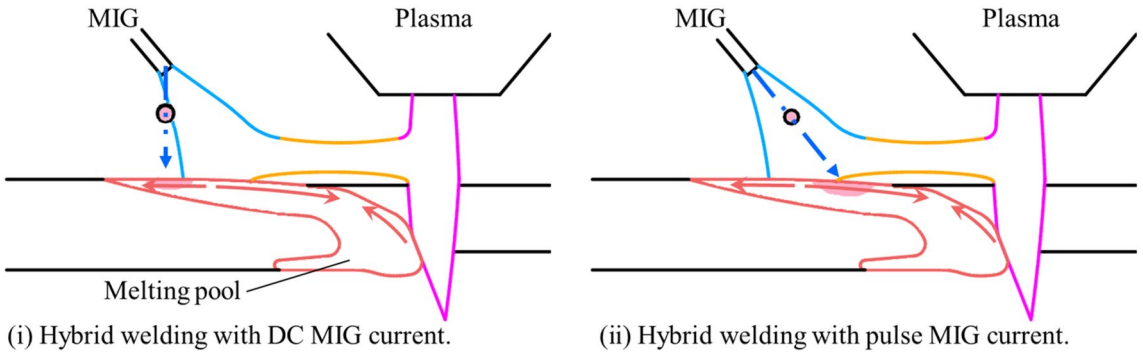

Fig. 7 Schematic of metal transfer position onto the weld pool surface for DC-MIG current and pulse-MIG current during plasma-MIG hybrid welding

Figure 5 shows the arc appearances and expected current paths for DC-MIG current and pulse-MIG current during plasma-MIG hybrid welding. In the case of DC-MIG current, the plasma arc and MIG arc were continuously connected due to the arc coupling to form a direct current path between them. According to this connection, MIG current was pulled forward and the electromagnetic force acting on the droplet neck became asymmetric to apply stronger downward force to it. As a result, the droplet was transferred downward as presented in Fig. 4. Figure 5b shows the image at the peak duration of pulse-MIG current. As found by Ishida et al. [11], the arc coupling occurs only in the upslope duration of pulse-MIG current. Therefore, MIG arc and its current path had almost axisymmetric distributions. Thus, the electromagnetic field was applied to the droplet neck also axisymmetrically, so the droplets were transferred along the wire axis.

Figure 6 shows the bead appearances, cross-sections, and Ni element distributions for DC-MIG current and pulse-MIG current. The bead appearances indicate that a full penetration was obtained, achieving the welding successfully for both conditions, even though the plasma current and MIG current in pulse-MIG current condition were much lower than those in DC-MIG current condition. The distributions of Ni element on the cross-sections were also measured by an electron probe micro analyzer (EPMA). As presented in Table 2, the content of Ni element was negligibly low in the base metal but high in the wire. Although a high content region was seen only in the upper half for DC-MIG current, it reached to almost the bottom surface for pulse-MIG

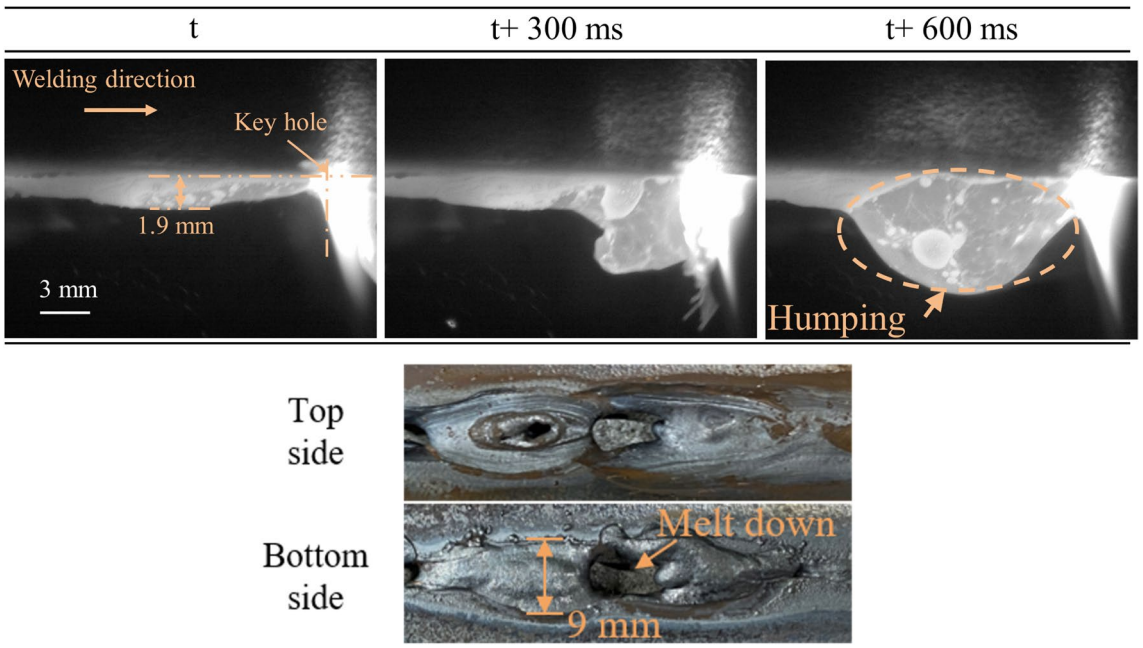

Fig. 8 An example of time sequential images of bottom side weld pool with humping and resultant weld bead for DC-MIG current

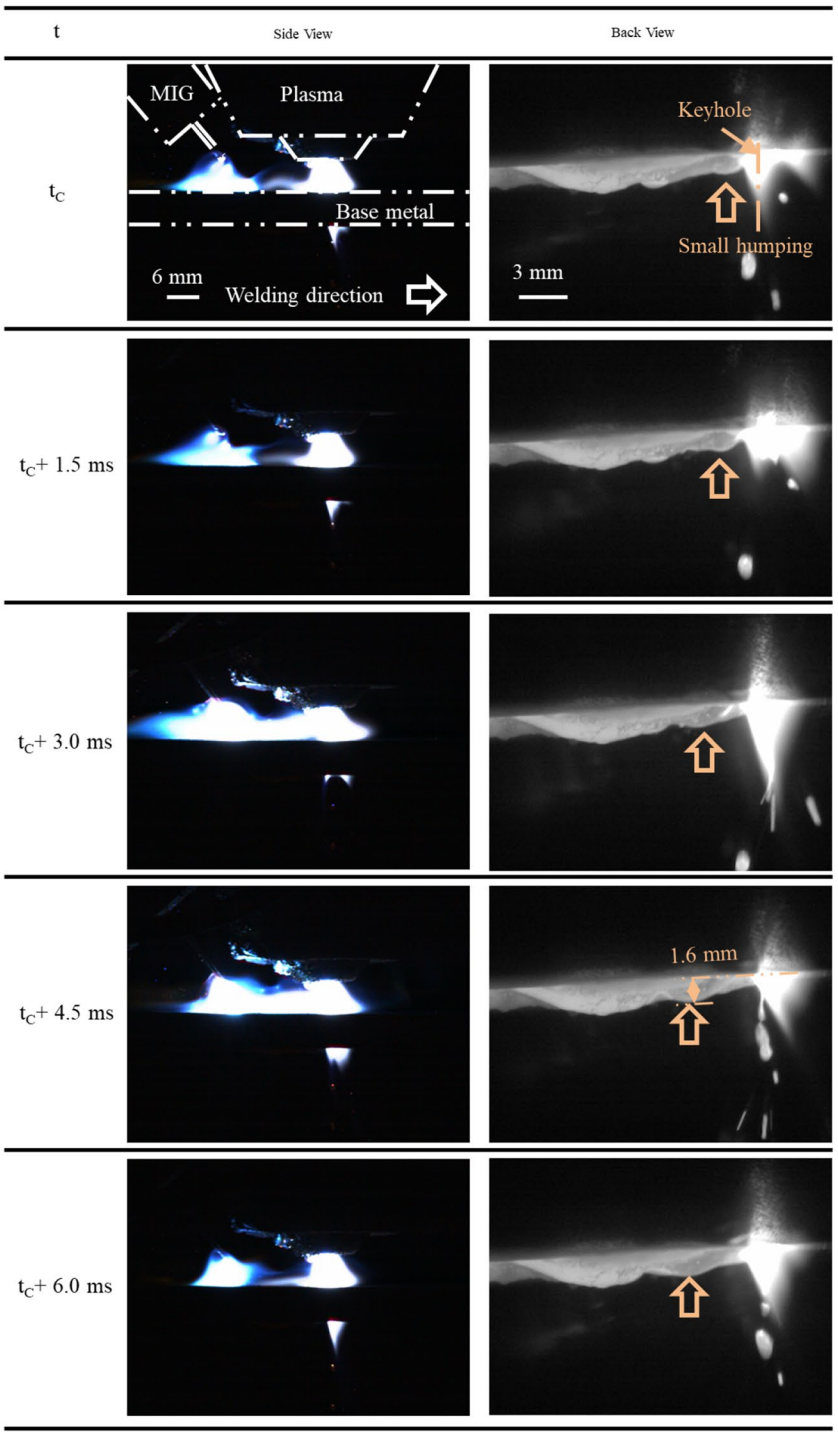

Fig. 9 Time sequential images of arc appearance and bottom side weld pool for pulse-MIG current

current. In addition, it can be seen that the weld pool is formed asymmetrically with respect to the weld line for DC-MIG current. This is considered to be caused by the unstable droplet detachment from MIG wire due to the axisymmetric electromagnetic force acting on the droplet neck.

Figure 7 shows the schematic of metal transfer position onto the weld pool surface for DC-MIG current and pulse-MIG current during plasma-MIG hybrid welding. Wu et al. found that many eddies are formed in weld pool of plasma-MIG hybrid welding, because both the plasma arc and MIG arc provide complex driving forces to the weld pool [13, 14]. In the weld pool behind keyhole, the backward flow (counter-clockwise eddy) is formed around the top surface due to the plasma shear force. Under the MIG arc, the forward and backward flows (clockwise and counter-clockwise eddies) are formed near the top surface mainly due to the

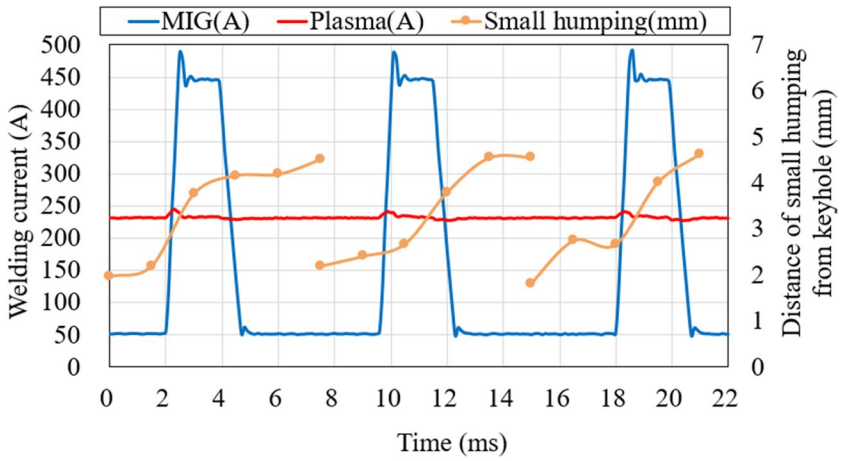

Fig. 10 Current waveform of plasma-MIG hybrid welding and distance of small humping from keyhole for pulse-MIG current

Marangoni force. The heat transport in weld pool is primarily governed by these weld pool flows. It is generally known that the temperature of droplet is much higher than that of weld pool and the heat input brought by droplets to the weld pool accounts for about 40% of total heat input in MIG welding [18]. When the droplet transferred to the weld pool region with the backward flow such as the DC-MIG current case, the heat is transported to the weld pool end, not contributing to increase the penetration depth. However, when the droplet is transferred to that with the forward flow such as the pulse-MIG current case, the heat is transported to the bottom side together with the counter-clockwise eddy behind the keyhole, strongly contributing to increasing the penetration depth. In the optimum condition of plasma welding used in this paper, the counter-clockwise eddy is formed behind the keyhole. However, the direction and magnitude of eddy are possible to change depending on the welding condition through variation of the driving force balance [19, 20]. This change is thought to also affect the heat transport by the droplet.

Consequently, it is found that the effect of MIG current waveform on penetration depth is significant because the heat transport in weld pool dramatically changes.

3.2 Effect of MIG current waveform on bottom side bead formation

Figure 8 shows an example of time sequential images of the bottom side weld pool with humping and the resultant weld bead for DC-MIG current. In the case of laser-MIG hybrid welding, it is known that a humping bead on the bottom surface tends to occur when the heat transport to bottom side in weld pool is not sufficient, because the size of bottom side weld pool is small to accumulate the molten metal behind the keyhole [13]. In the plasma-MIG hybrid welding, a similar phenomenon is also seen especially for DC-MIG current as in Fig. 8, since the heat transport to the bottom side is

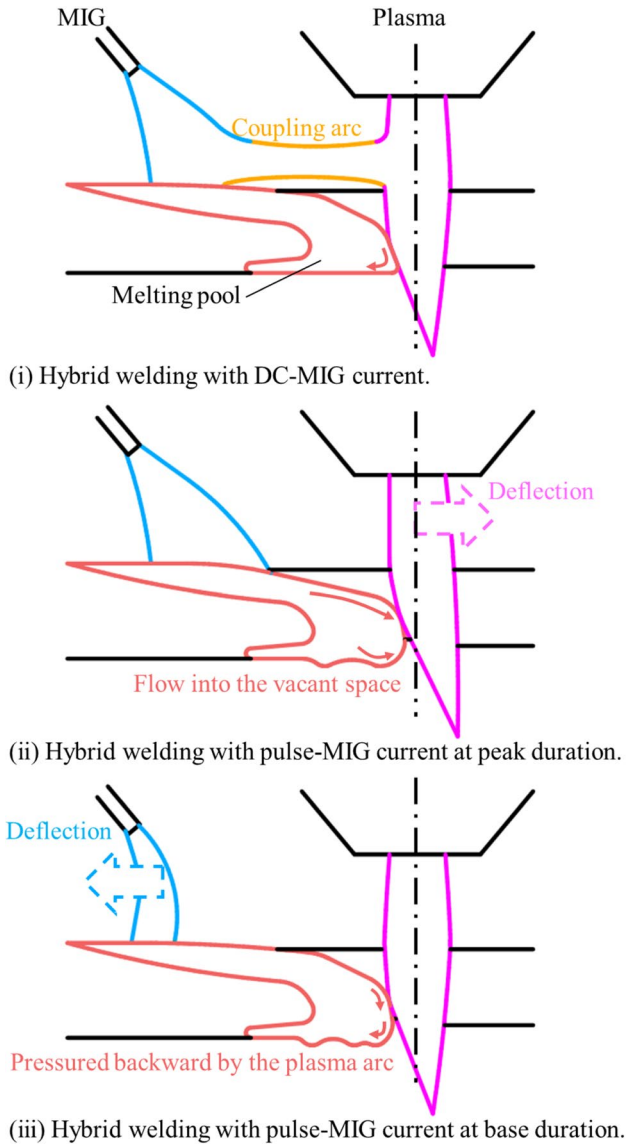

Fig. 11 Schematic diagram of the mechanism of small humping movement

smaller as described above. It strongly limits the range of suitable welding conditions.

Figure 9 shows the time sequential images of the arc appearance and bottom side weld pool for pulse-MIG current. In the case of pulse-MIG current, the arc coupling periodically occurs to cause oscillation of the efflux plasma outflowing downward through the keyhole. Around time from t_c + 1.5 to 3.0 ms, the efflux plasma was deflected forward due to the strong electromagnetic interaction to MIG current during upslope duration. In the bottom side weld pool images, a small humping (denoted by an orange arrow) was seen to move from the region behind keyhole to the weld pool end synchronized with the efflux plasma oscillation.

Figure 10 shows the current waveform of plasma-MIG hybrid welding and the distance of small humping from keyhole for pulse-MIG current. The period of pulse-MIG current was 7.6 ms, so three cycles of current waveform are presented. In the observation of the bottom side weld pool, occurrences of small humping were seen three times. From a result, it was found that small humping was formed around the center of base current duration and moved backward. Especially, it was accelerated around the pulse peak duration.

Figure 11 shows the schematic diagram of the mechanism of small humping movement. In the case of DC-MIG current, the arc coupling between plasma and MIG arcs continuously occurs, so the plasma arc position is stable. On the other hand, in the case of pulse-MIG current, the plasma arc position changes depending on the current waveform. In the peak current, the plasma arc is deflected forward to expand the weld pool forward. Then, the plasma arc returns the original position to push the weld pool backward in the base current. Therefore, the weld pool behind the keyhole periodically oscillates according to change in the plasma arc position. It transports the molten metal on the bottom surface backward. Consequently, the accumulation of molten metal behind keyhole is prevented to suppress the humping bead formation.

4 Conclusion

The main results of this study are summarized as follows:

1) The effect of arc coupling for DC-MIG current and pulse-MIG current on the heat transport in weld pool and the humping bead formation was for the first time clarified.
2) The droplets after detachment from wire were transferred to weld pool surface under the wire tip for DC-MIG current, while those were transferred along the wire axis to weld pool surface behind the keyhole for pulse-MIG current.
3) When the droplet is transferred to the weld pool region with the forward flow such as the pulse-MIG current case, the heat is transported to the bottom side together with the counter-clockwise eddy behind the keyhole, strongly contributing to increasing the penetration depth.
4) In the case of pulse-MIG current, the plasma arc is oscillated due to the arc coupling. According to this oscillation, the accumulation of molten metal behind keyhole is prevented to suppress the humping bead formation.

Funding Open Access funding provided by Osaka University. This work was supported by JSPS KAKENHI (Grant Number JP21K04710), the Project on Design & Engineering by Joint Inverse Innovation for Materials Architecture (DEJI2MA) from the Ministry of Education, Culture, Sports, Science and Technology (MEXT), and an OU Master Plan Implementation Project promoted under Osaka University.

Declarations

Ethics approval The authors state that the present work is in compliance with ethical standards.

Consent to participate All the authors listed have approved the manuscript and consented to participate.

Consent for publication All the authors listed have approved the manuscript and consented for publication.

Conflict of interest The authors declare no competing interests.

References

1. Shen J, Agrawal P, Rodrigues TA, Lopes JG, Schell N, He J, Zeng Z, Mishra RS, Oliveira JP (2023) Microstructure evolution and mechanical properties in a gas tungsten arc welded Fe42Mn28Co10Cr15Si5 metastable high entropy alloy. Mater Sci Eng A 867:144722
2. Lopes JG, Agrawal P, Shen J, Schell N, Mishra RS, Oliveira JP (2023) Evolution of microstructure and mechanical properties in gas tungsten arc welded dual-phase Fe50Mn30Co10Cr10 high entropy alloy. Mater Sci Eng A 878:145233
3. Vollertsen F, GrÜnenwald S, Rethmeier M, Gumenyuk A, Reisgen U, Olschok S (2010) Welding thick steel plates with fiber lasers and GMAW. Weld World 54:62–70

4. Cao X, Wanjara P, Huang J, Munro C, Nolting A (2010) Hybrid fiber laser – arc welding of thick section high strength low alloy steel. Mater Des 32:3399–3413
5. Pan Q, Mizutani M, Kawahito Y, Katayama S (2016) High power disk laser-metal active gas arc hybrid welding of thick high tensile strength steel plates. J Laser Appl 28:012004
6. Skowro´nska B, Chmielewski T, Gola´nski D, Szulc J (2020) Weldability of S700MC steel welded with the hybrid plasma + MAG method. Manuf Rev 7:4
7. Yuji T, Tashiro S, Kinoshita H, Yasui K, Bouno T, Wu Z, Wu D, Poonthong W, Rahman SA, Mamat SB, Tanaka M (2024) An investigation on plasma-MIG hybrid welding process of thick plate aluminum. J Adv Join Process 9:100188
8. Wang W, Yamane S, Wang Q, Shan L, Zhang X, Wei Z, Yan Y, Song Y, Numazawa H, Lu J, Xia Y (2023) Visual sensing and quality control in plasma MIG welding. J Manuf Process 86:163–176
9. Jiang F, Li W, Xu B, Cheng W, Zhang G, Ma X, Chen S (2024) Variable polarity plasma arc welding: process development and its recent developments of detecting, modeling, and controlling. J Manuf Process 114:1–17
10. Tashiro S (2024) Interaction mechanism of arc, keyhole, and weld pool in keyhole plasma arc welding: a review. Materials 17:1348
11. Ishida K, Tashiro S, Nomura K, Wu D, Tanaka M (2022) Elucidation of arc coupling mechanism in plasma-MIG hybrid welding process through spectroscopic measurement of 3D distributions of plasma temperature and iron vapor concentration. J Manuf Process 77:743–753
12. Wu D, Tashiro S, Wu Z, Tanaka M, Nomura K, Hua X (2020) Interactive phenomena in Hybrid KPAW–GMAW-P. Weld J 99:146s–55s
13. Wu D, Tashiro S, Wu Z, Nomura K, Hua X, Tanaka M (2020) Analysis of heat transfer and material flow in hybrid KPAW-GMAW process based on the novel three dimensional CFD simulation. Int J Heat Mass Transf 147:118921
14. Wu D, Ishida K, Tashiro S, Nomura K, Hua X, Ma N, Tanak M (2023) Dynamic keyhole behaviors and element mixing in paraxial hybrid plasma-MIG welding with a gap. Int J Heat Mass Transf 200:123551
15. Yu J, Wang B, Zhang H, Wang Q, Wei L, Chen P, He P, Feng J (2020) Characteristics of magnetic field assisting plasma GMAW-P. Weld J 99:25s–38s
16. Yu J, Zhang H, Yang X, Teng Y, Wang Q, Wei L, He P, Zhang W (2021) Arc characteristics and welding process of magnetic field assisting plasma-GMAW-P. Weld J 100:1–12
17. Frostevarg J (2018) Factors affecting weld root morphology in laser keyhole welding. Opt Lasers Eng 101:89–98
18. Tsujimura Y, Tanaka M (2012) Numerical simulation of heat source property with metal vapor behavior in GMA welding. J Japan Weld Soc 30:68–76
19. Nguyen AV, Tashiro S, Ngo MH, Bui HV, Tanaka M (2020) Effect of the eddies formed inside a weld pool on welding defects during plasma keyhole arc welding. J Manuf Process 59:649–657
20. Nguyen AV, Wu D, Tashiro S, Tanaka M (2019) Undercut formation mechanism in keyhole plasma arc welding. Weld J 98:204-s